INFRARED ATLAS CHARTS OF THE ECLIPSED MOON*

RICHARD W. SHORTHILL**
The Lunar Science Institute, Houston, Tex., U.S.A.

(Received 31 August, 1972)

Abstract. The objective of this atlas is to present the thermal response of the lunar surface observed during an eclipse of the Moon with accurate position data. The observations were made at a wavelength of 11 μm with an angular resolution of 10″, equivalent to 17 km at the disk center. Over a thousand thermally anomalous regions (hot spots) were detected. They cool more slowly than their environs and remain warmer than their environs during the umbral phase. In addition to these very localized hot spots some of the maria show thermal enhancements during the eclipse.

Fourty four charts make up this atlas which are identical in coverage and projection to the Lunar Atlas Charts (LAC)*** series. The charts are in the form of digital images of a normalized temperature difference which is particularly useful for studying regions of small thermal enhancements. Each increase of intensity corresponds to 4 K temperature increase. Grid lines are drawn every two degrees with tic marks each one-half degree. A brief outline of the observations and data reduction methods is given. The map construction techniques are described along with a discussion on how the atlas could be used.

The appendix is a list of the published infrared atlantes. These include isothermal contour maps and images of the day-time, eclipsed and night-time Moon, and catalogues of thermal anomalies of the eclipsed and night-time Moon.

1. Observations

The total eclipse of the Moon was observed from the eastern desert region of Egypt 1964, December 19, using the 74-in. Kottamia telescope of the Helwan Observatory (Samaha, 1967). The circumstances of this eclipse are given in Table I. Measurements were made on the illuminated Moon starting 17 December, 1964, to verify that all equipment and telescope systems were functioning. A full Moon observation (phase angle $-2°16'.12$) was completed 30 min before first contact followed by eight observations during the course of the eclipse (penumbra, umbra, and post-penumbra). The data used for this atlas were obtained from the measurements during the umbral phase between $2^h10^m.3$ and $2^h27^m.3$ UT. This particular observation was chosen because the average brightness temperature of the lunar surface was higher than during subsequent observations in umbra. Also as observations continued during the umbral phase the limb temperatures decrease rapidly and approached the detectability limit of the infrared system making it impossible to map the limbs completely.

* Paper dedicated to Professor Harold C. Urey on the occasion of his 80th birthday on 29 April, 1973. A portion of the research reported in this paper was done while the author was a Visiting Scientist at The Lunar Science Institute, which is operated by the Universities Space Research Association under Contract NSR-09-051-001 with the National Aeronautics and Space Administration. This paper is Lunar Science Institute Contribution No. 111.

** Usually at The Boeing Company, Space and Planetary Environments, Seattle, Wash. 98124, U.S.A.

*** This series of lunar charts were prepared by the United States Air Force Aeronautical Chart and Information Center, St. Louis, Missouri.

The Moon 7 (1973) 22–45.

TABLE I

Circumstances of the total lunar eclipse
December 19, 1964[a]

	d	h	m
Moon enters penumbra	19	00	01.3
Moon enters umbra	19	00	59.8
Total begins	19	02	07.8
Middle of eclipse	19	02	37.9
Total eclipse ends	19	03	07.9
Moon leaves umbra	19	04	16.0
Moon leaves penumbra	19	05	14.4

[a] American Ephemeris, 1964, p. 302

The focal plane scanner and detector system were originally built by the Boeing Scientific Research Laboratories for use at the Newtonian focus of the Mt. Wilson 60-in. telescope (Shorthill and Saari, 1965a). It was modified to give more than 200 contiguous traverses with a resolution of 10″ in the 10 to 12 μm wavelength band. Each traverse required about 5 s at a rate of 700″ per s. This rapid traverse motion was obtained with a lag screw driven by a reversible synchronous motor. A microswitch at each end of the traverse initiated the following turn-around sequence:

(a) A fiducial-marker signal was turned on and recorded for positional information.

(b) The traverse motor power was turned off. Disk brakes were applied to bring the scanner to a smooth stop.

(c) The advance motor was turned on, driving a second lag screw which advanced the photometer vertically one resolution element (equivalent to 10″).

(d) The brakes were then released and the traverse motor turned on in the opposite direction.

(e) After the traverse motor was up to speed (constant velocity) the fiducial-marker switch was turned off by the scanning motion and the photometer continued to scan.

(f) The fiducial-marker switch at the other extreme of the traverse was turned on and the sequence repeated. Each observation of the lunar disk required slightly more than 200 traverses and took about 17 min to complete. An example is shown in Figure 1. During the turn-around sequence when the photometer aperture was well off the lunar disk at the start and finish of each traverse, sky background readings were obtained. All these data were tape recorded and simultaneously monitored with a chart recorder and loud speaker as illustrated in Figure 2.

The telescope tracking motion was set near lunar rate in right ascension. A dual channel pulsing circuit with variable pulse width and repetition rate was used to obtain the true lunar rate in both right ascension and declination. An 8-in. reflecting telescope mounted on the side of the main telescope was used for monitoring the position and tracking rates. If corrections were required they were made during the turn-around sequence between (b) and (d) to minimize position errors during the scanning sequence.

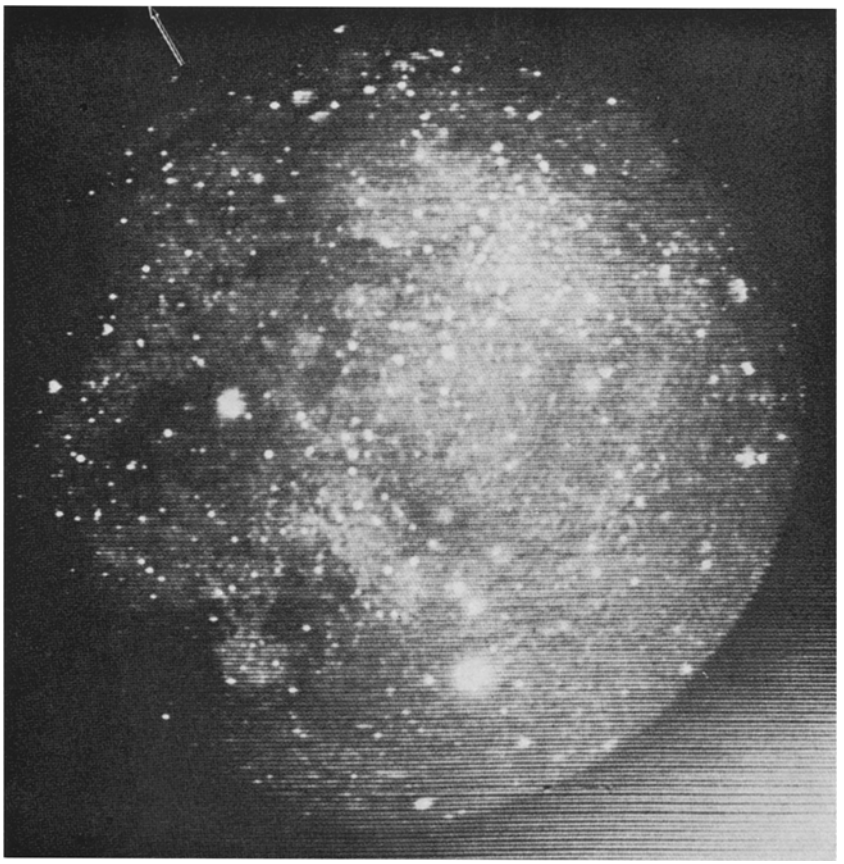

Fig. 1. Infrared image of the eclipsed Moon observed from $2^h10^m.3$ to $2^h27^m.3$ UT, 1964, December 14. Note the bright region in the lower right hand corner which is caused by emission from the telescope structure. The arrow indicates north.

2. Reduction of Data

After returning to the laboratory the data from the analog tapes were digitized, using a custom built Epsco A/D Converter at 312.5 samples per s per channel. The infrared channel was sampled alternately with the fiducial-marker channel which furnished the time base by indicating the start and stop time for each traverse, the elapsed time for each traverse, and the time on the sky during the turn-around sequence. Many steps were required in the initial data reduction (Saari and Shorthill, 1967) several will be described briefly here.

A. FILTER ROUTINE

The original analog signals were smoothed by the R-C network in the infrared photometer and then, to eliminate the chopping noise, passed through a 200 Hz Bessel (active) filter before being recorded on tape. Power spectral analysis of similar mea-

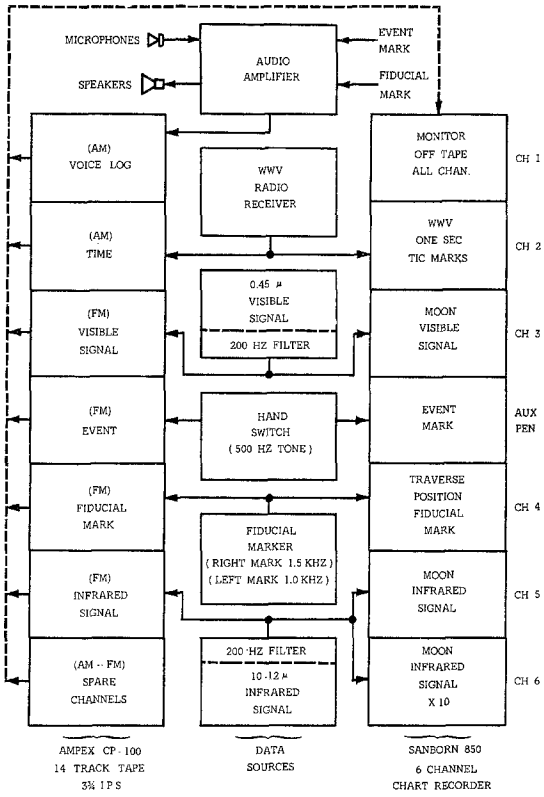

Fig. 2. Block diagram of the equipment used for observing the infrared emissions and visible reflections from the Moon.

surements taken with this system on the Mt. Wilson 60-in. telescope showed that the information was concentrated in the frequency region below 30 Hz. Thus a numerical (digital) filter was constructed having a nominal 41.5 Hz cutoff frequency and a 62.5 Hz termination frequency and applied to the digital data. Following this process the data were checked against a set of calibration signals on the original tapes to remove any nonlinearity in the record-reproduce-digitize sequence.

B. BACKGROUND RADIATION CORRECTION

The infrared photometer receives radiation from several sources other than the Moon such as the sky, the mirrors and the telescope support structures. It is necessary to subtract off these background radiation sources to obtain the net signal from the Moon. Signals from the illuminated Moon were relatively large compared to the signals from the sky alone. It was sufficient to subtract the average of the sky signals at the start and end of each traverse to obtain the net lunar signal (Saari and Shorthill, 1967). During the eclipse, however, when the amplifier gain was increased the non-uniform background radiation over the focal plane became significant and the earlier procedure could not be used. Figure 1 is an image of the analog data showing this

non-uniform background (greatest in the lower right-hand corner). An observation was made on the sky alone, that is, the scanner was turned on and a map of the background radiation in the focal plane was made. This background radiation map was normalized to the eclipse observation using the sky values obtained during the turn around sequences and subtracted from the eclipse observations (Shorthill *et al.*, 1970).

C. CALIBRATION

The calibration of the infrared photometer takes into consideration the total mass of air and water vapor for the different eclipse and full Moon observations and the sensitivity of the telescope and photometer (detector and amplifier) system. Observations made of the full Moon just preceding the eclipse were used to obtain the brightness temperature of the subsolar point taking into account conduction into the surface, local albedo, and directional effects. Then a calibration for the center of the disk was determined for each observation during the eclipse. A detailed description is given elsewhere (Saari and Shorthill, 1967; Shorthill *et al.*, 1970).

D. LINE-SHIFT ROUTINE

When the original analog data were smoothed with an R-C filter, a phase shift was introduced causing a horizontal displacement of an entire traverse line by several data points. Since successive traverse lines scanned the Moon in opposite directions, the filter smoothed successive traverse lines in opposite directions. The net effect, therefore, was that every other traverse was shifted resulting in a serrated edge. This was corrected by choosing a certain signal level near the brightest limb and computing the every-other-traverse 'line-shift' necessary to produce a smooth circular limb.

E. LOCATION

When an observation was made neither the position nor the rotation of the raster pattern relative to the disk of the Moon were known. Contours of the full Moon data were constructed from both the infrared and the visible wave length signals. A conversion from scanner coordinate system (i.e., traverse line number and data point number) to a selenographic grid system was determined so that grid lines could be constructed as shown in Figures 3 and 4 (Saari and Shorthill, 1967). The method consisted of first determining the scanner coordinates of a number of small bright identifiable features. Next a least-squares fit was made between the calculated librated selenographic coordinates for these features and the scanner coordinates, and an analytic conversion formula generated. The formal rms error using 36 features was 2.1″ ($\frac{1}{4}$ the resolution element). Similar procedures were followed with the eclipse observations using the full Moon contour charts as a guide to identify features on the eclipse isothermal contour charts.

3. Chart Construction

An *Isothermal and Isophotic Atlas of the Moon* was published by Saari and Shorthill

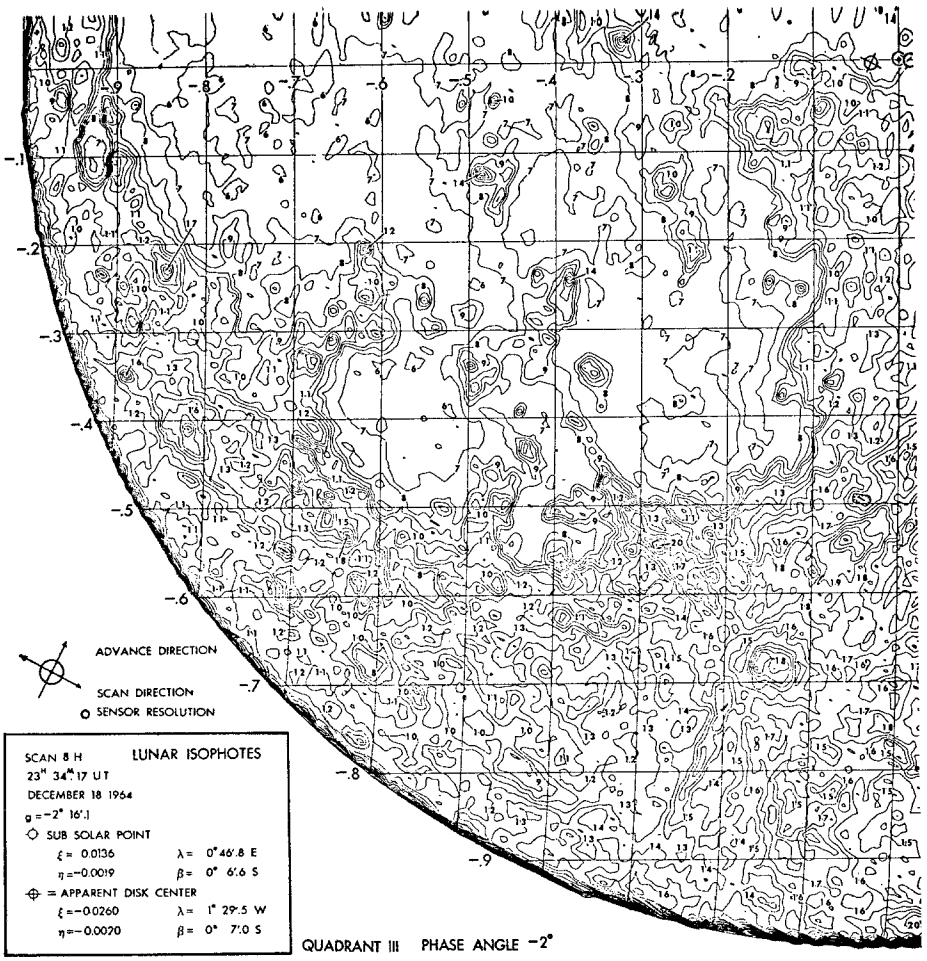

BRIGHTNESS CALIBRATION DATA

Contour Number	Brightness Value b	Contour Number	Brightness Value b
4	22.22	20	111.12
5	27.78	21	116.68
6	33.34	22	122.23
7	38.89	23	127.79
8	44.45	24	133.34
9	50.00	25	138.90
10	55.56		
11	61.12		
12	66.67		
13	72.23		
14	77.78		
15	83.34		
16	88.90		
17	94.45		
18	100.01		
19	105.56		

Fig. 3. Isophotic contours of the southwest quadrant of the full Moon. The integral brightness of the disk at zero phase was equated to a value of 100.

(1967). This consisted of a series of contours for the illuminated portion of the lunar disk. Librated standard orthographic grid lines (ξ, η) were constructed by the least

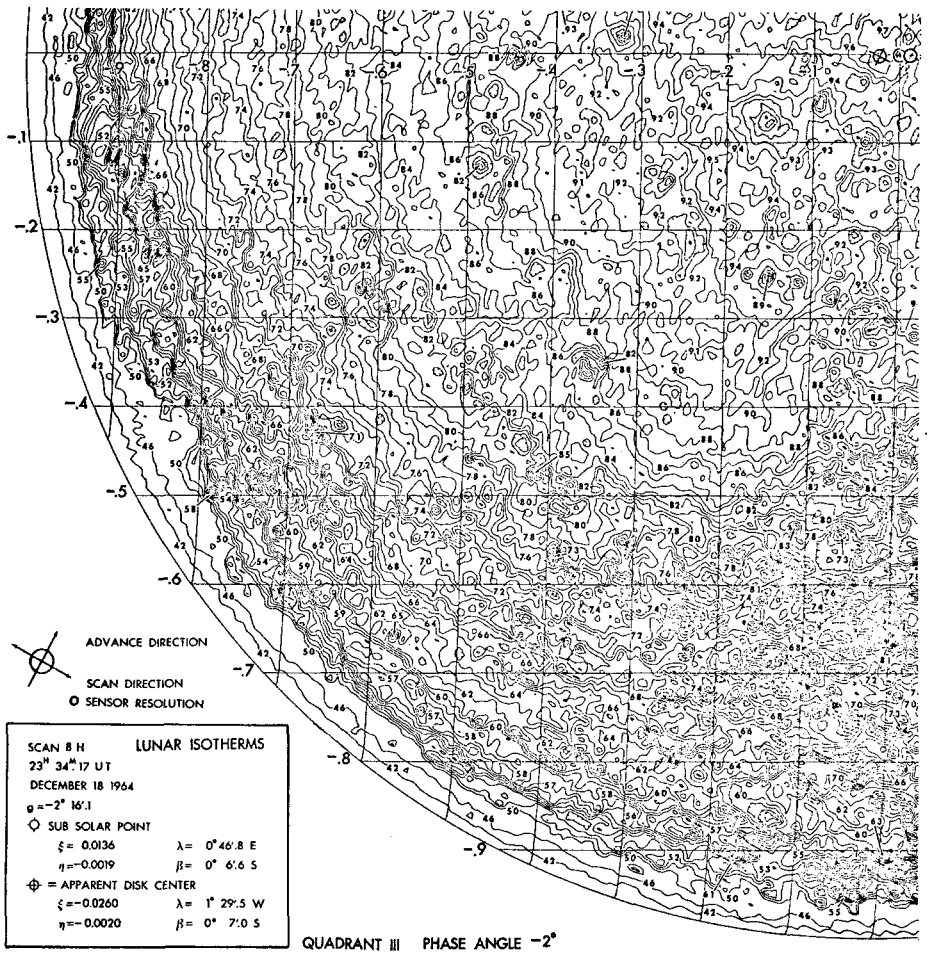

THERMAL CALIBRATION DATA

Contour Number	Temperature °K	Contour Number	Temperature °K	Contour Number	Temperature °K	Contour Number	Temperature °K	Contour Number	Temperature °K
.75	161.7	34	304.1	58	346.2	74	369.3	90	390.2
2	183.9	36	308.2	59	347.8	75	370.7	91	391.4
4	203.7	38	312.1	60	349.3	76	372.1	92	392.6
6	217.3	40	315.9	61	350.8	77	373.4	93	393.9
*10	237.4	42	319.5	62	352.3	78	374.7	94	395.1
12	245.4	44	323.1	63	353.8	79	376.1	95	396.3
14	252.7	46	326.7	64	355.2	80	377.4	96	397.5
16	259.3	48	330.1	65	356.7	81	378.7	97	398.7
18	265.4	50	333.4	66	358.1	32	380.0	98	399.9
20	271.1	**51	335.1	67	359.6	83	381.3	99	401.1
22	276.5	52	336.7	68	361.0	84	382.6	100	402.3
24	281.7	53	338.3	69	362.4	85	383.9	101	403.5
26	286.5	54	340.0	70	363.8	86	385.1		
28	291.2	55	341.5	71	365.2	87	386.4		
30	295.7	56	343.1	72	366.6	88	387.7		
32	300.0	57	344.7	73	368.0	89	388.9		

*Note level Number 8 not contoured.

**Note change in levels contoured from Number 51 on.

Fig. 4. Isothermal contours of the southwest quadrant of the full Moon. The isophotic contours in Figure 3 were obtained at the same time.

squares fit method for the maps (see Figures 3 and 4). Similar isothermal contour charts were prepared for the eclipse data (see Figure 5).

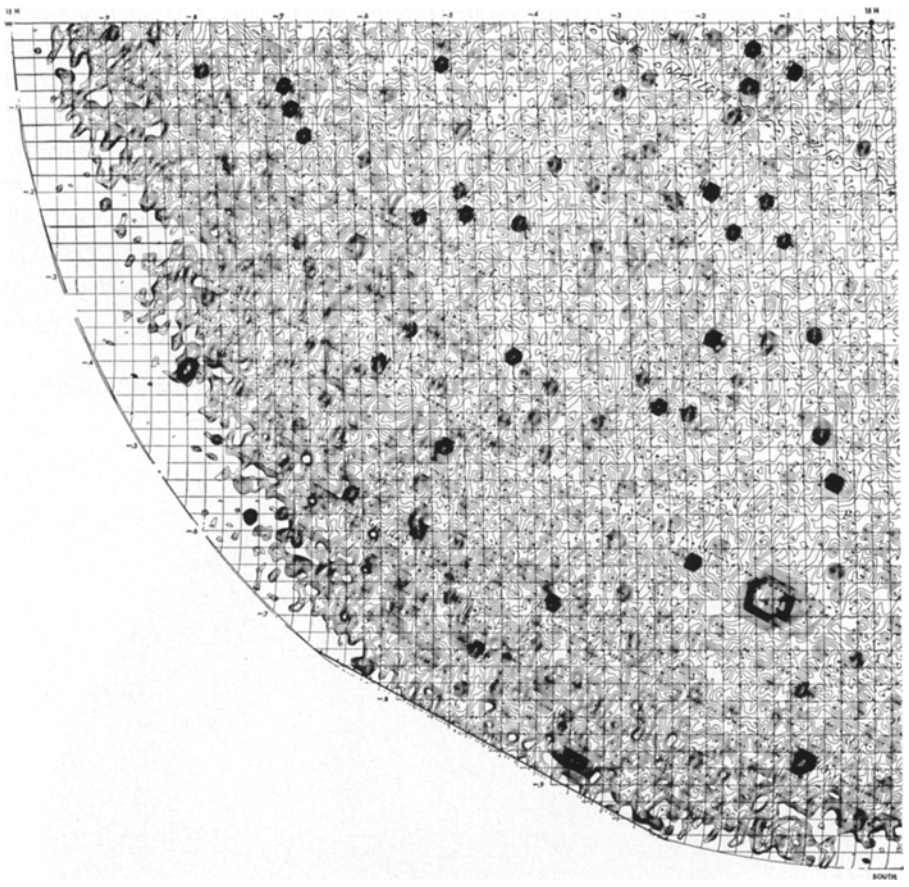

Fig. 5. Isothermal contours of the eclipsed Moon, 1964, December 19, between 2^h54^m3 and 3^h02^m8 UT. The absence of contours on the southwest limb results when the brightness temperature falls below 140 K.

The isothermal contour charts of the eclipsed Moon shown in Figure 5 are useful in demonstrating the variations of thermophysical properties over the surface and for studying localized features. It is, however, difficult to compare widely separated areas during an eclipse on a more or less equal basis. This difficulty arises from three causes: (1) At full Moon there is an observed 80 K variation in temperature from the subsolar point ($\sim$400 K) to the limb ($\sim$320 K). As the lunar surface cools during an eclipse this initial difference, albeit reduced, is still maintained. (2) The shadow passes approximately from West to East during an eclipse resulting in an asymmetry in the cooling conditions since the local temperature is a function of time in the shadow. (3) Successive traverses advanced across the lunar disk from the south-west to the north-east. Since an observation requires 17 min, features on traverse number one have a difference in cooling time of 17 min compared to features observed on traverse number 200. To remove these three difficulties a new map was constructed in the

form of a set of differential values from an *unenhanced base*. The *unenhanced base* corresponds to the 'average upland region' which observationally reaches the lowest temperature range at any given time during an eclipse and from which thermal enhancements (hot spots), where they exist on these upland regions, were excluded. An analytical expression of the base was developed from observational data for the uplands using a curve fitting procedure. The unenhanced base temperatures were normalized to the initial local (full Moon) values. Next the actual observed eclipse temperatures were normalized to the initial (full Moon) values. The difference from the base formed a new differential map as shown in Figure 6. The *Infrared Atlas Charts of the Eclipsed Moon* were constructed using this new data set for the 44 LAC quadrangles from $\pm 70°$ long. and $\pm 64°$ lat.

To aid in the analysis the infrared data the contours were manually transferred to

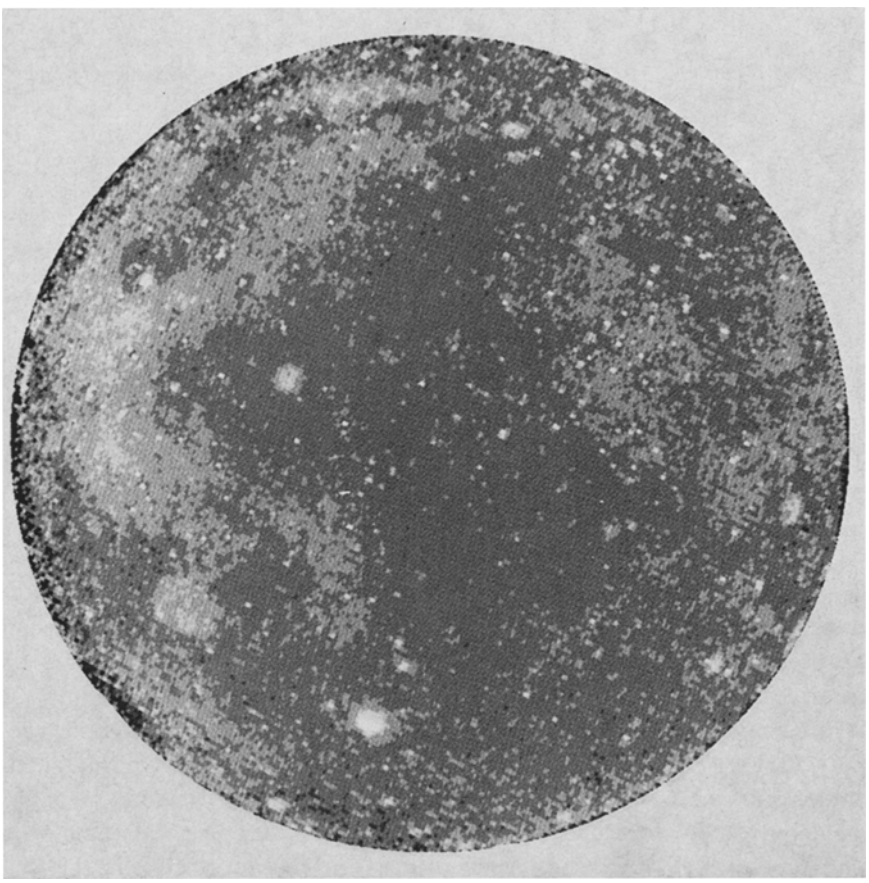

Fig. 6. Digital image of the normalized temperature difference in 10 K increments above the unenhanced base. The original observations were obtained 1964, December 19, between 2^h10^m3 and 2^h37^m3 UT. The data have been transformed to the mean librarion with north at the top. The small bright areas are thermal anomalies which have been interpreted as the effect of an excess in the number of boulders. (Compare with Figure 1.)

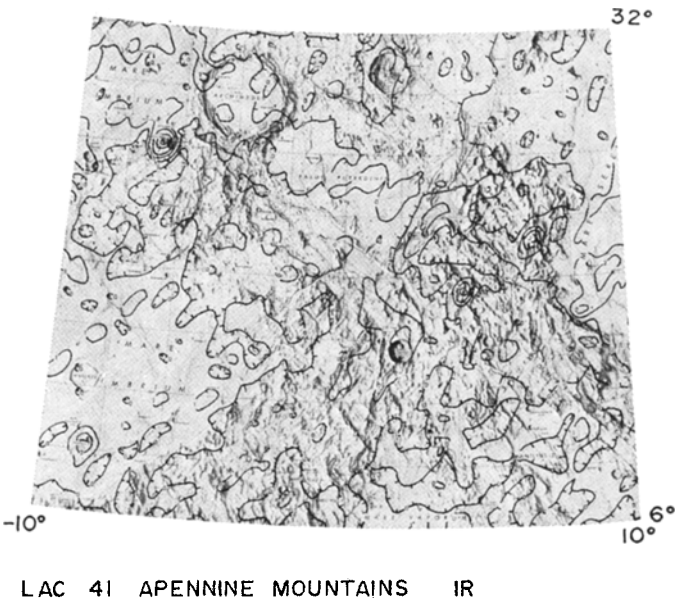

Fig. 7. Isocontours of the normalized temperature difference above the unenhanced base plotted on LAC 41. Each level corresponds to 4 K above the base. (Compare with Figure 8.)

several LAC charts (see Figure 7). Direct comparisons (i.e., overlays) with lunar features and the Lunar Orbiter and Apollo photography was now possible. Correlation with other remote-sensed data (i.e., radar, colorimetry) is facilitated. This method however required much time and is subject to the usual errors during the manual transfer process. Real improvement would be made if the infrared data and other data were displayed at the same projection and scale. The 70-cm radar data of Thompson (1972) were already computorized for variable-projection display at the Image Processing Laboratory (IPL) of the Jet Propulsion Laboratory.

The infrared eclipse data were formated for the IPL. During the image making procedure the oscilloscope beam is held on at each position for a time corresponding to the infrared signal strength. The face of the oscilloscope is photographed during this process until a chart is made. It is first necessary, however, to transform the original infrared observations to the mean libration. Charts for each LAC quadrangle are constructed for both the infrared and the 70-cm data at identical scale and projection. Figure 8 shows the infrared and 70-cm radar images for LAC 41 Montes Apenninus at the same scale and projection. A section of the 4-cm radar image of the same LAC is also shown.

Severe distortions in the infrared data are encountered at a radial distance greater than 70° as illustrated in a Mercator projection of LAC 99 Humboldt 70° to 90°E; 16° to 32°S in Figure 9. This distortion is caused by the foreshortening and certain computer-generated effects during the transformation of the original data from orthographic to Mercator projection. The blank area from about 88° to 90°E results

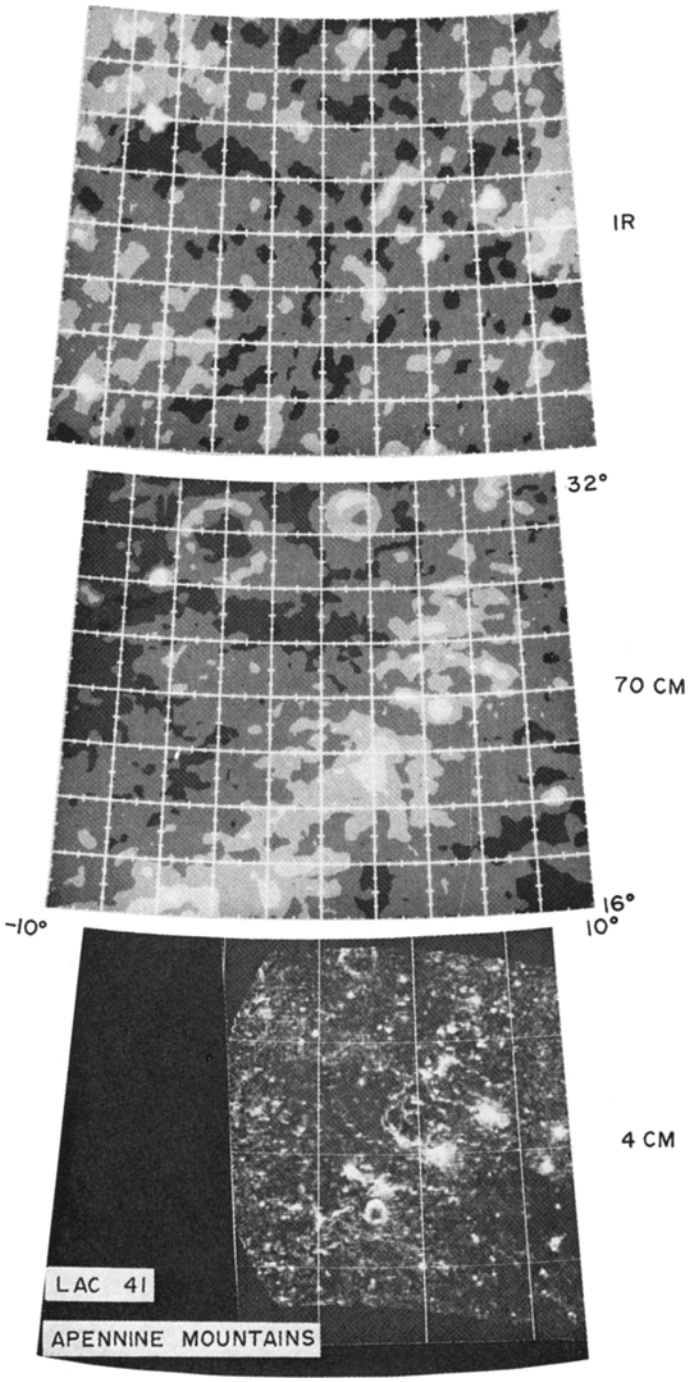

Fig. 8. Three images of LAC 41. The IR normalized temperature differences in 4 K increments above the unenhanced base. The depolarized 70-cm radar back scatter where adjacent brightness levels indicates a ratio of 1:2 in radar echo strength (Thompson, 1972). The depolarized 4-cm radar back scatter where adjacent brightness levels indicates a ratio of 1:2 in radar echo strength (Zisk *et al.*, 1971). The resolution is about 15 km for the IR and 70-cm images while it is 2 km for the 4-cm image.

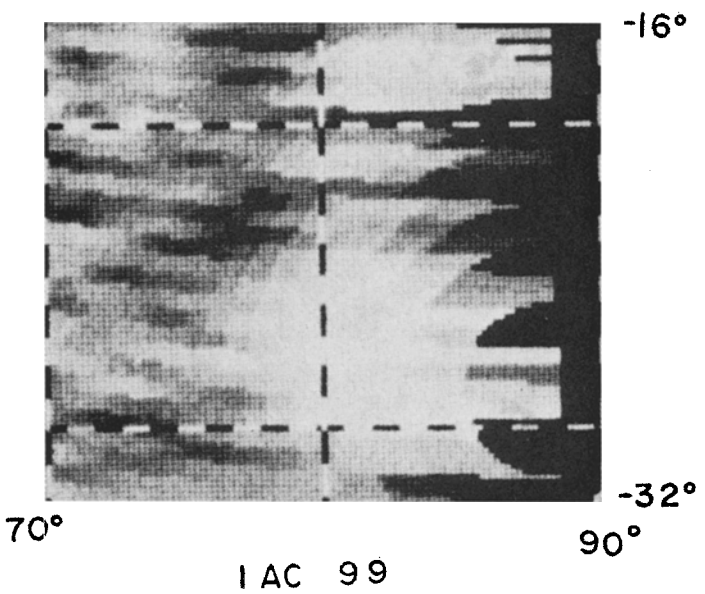

Fig. 9. Infrared Atlas Chart (IAC) 99 Humboldt 16° to 32° S, 70° to 90° E. Distortions are caused by the computor transformation from orthographic to Mercator projections.

from the eastern libration of the Moon during the observations. The serrated east edge is caused by magnification of the electronic RC filtering effect explained in Section 2. The dark regions less than 88° E long. result because the temperatures were at or below the noise level of the infrared photometer system.

4. Discussion

The reason for measuring the infrared emission from the Moon is to increase our knowledge of the physical character of the lunar surface (Shorthill, 1972). The differential cooling rates of lunar surface materials during the night-time and eclipse reveal certain physical properties of the surface. The particle size distribution in the soil, the local surface roughness, the distribution of boulders on the surface all affect the cooling rates. While the night-time measurements may show more thermal contrast they are difficult to obtain because of the low surface temperatures (<100 K). Many hours are required to map the thermal emission of the night-time lunar surface (Mendell and Low, 1970; Murray and Wildey, 1964; Allen, 1971a, b). Mapping of the eclipsed Moon can be accomplished in a shorter time because the average surface temperature is much higher (>160 K).

The eclipse infrared measurements (Shorthill *et al.*, 1960; Saari and Shorthill, 1963; and Shorthill and Saari, 1965b), have been interpreted in terms of the thermophysical properties of the average lunar soil (Winter, 1966a, b, 1967; Winter and Saari, 1969)

and the thermophysical properties of surface rocks (Roelof, 1968; Winter, 1970; Allen, 1971a; and Shorthill and Saari, 1972).

Recently a series of comparison studies were made to find correlations between the lunar eclipse infrared data, the 3.8-cm lunar radar backscatter data, the 70-cm lunar radar backscatter data, the lunar geological photo interpretations and the surface expressions found on the Lunar Orbiter and Apollo high resolution photography (Thompson *et al.*, 1970; Zisk *et al.*, 1971; Shorthill *et al.*, 1972; Zisk *et al.*, 1972). The correlation parameters were related to the physical properties of the surface and subadjacent layers. For these studies it was found very useful to have charts or maps of the various data sets at the same projection and scale (see Figure 8). It was easy then to locate common points for comparison and refer to the more detailed original data which in some cases were at a much finer resolution.

This information can be combined with many other data (i.e., colorimetry, magnetic) to improve the understanding of the processes that brought the Moon's surface to its present state and continues to influence its surface.

5. Infrared Atlas Charts

Approximately two-thirds of the Earth-visible surface is covered by the 44 Infrared

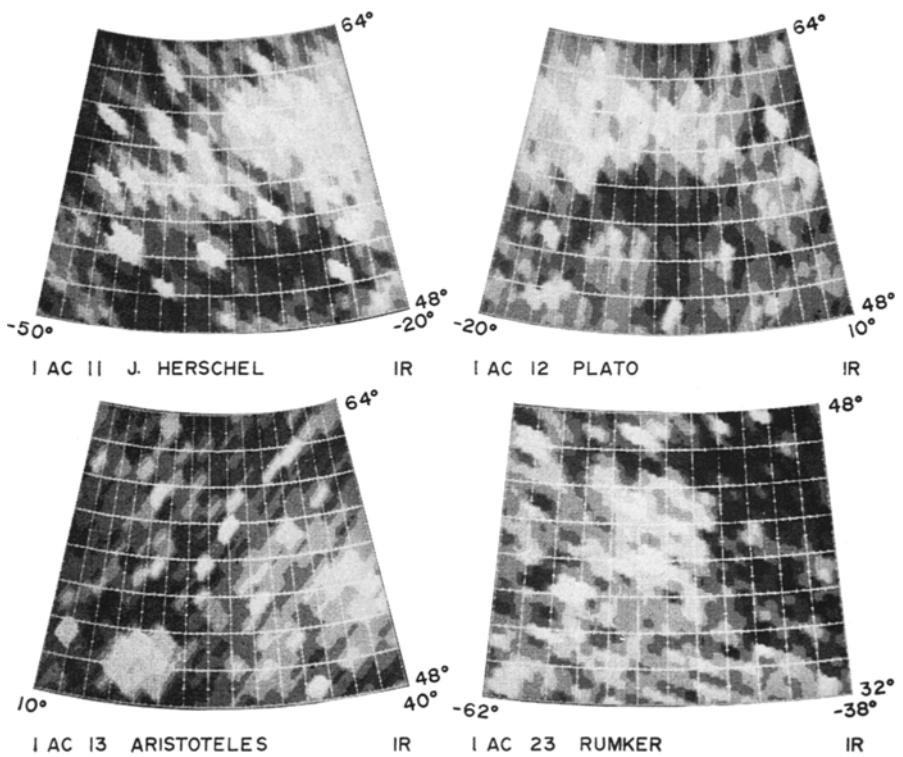

Plate A-I.

Atlas Charts (IAC). Each chart has the same coverage as the LAC series which is 16° in lat. and 30° in long. for ±(48° to 64°) lat., 24° for the ±(32° to 48°) lat. band and 20° for the 0° to ±32° lat. band. Each IAC carries the same name as the LAC series. Since the defining aperture of the infrared photometer was circular the resolution element is in general an elipse when projected on the lunar surface. For example, on the equator the minor axis of the elipse is 17 km north–south while the major axis varies from 44 km at 70° long. to 17 km at the disk center.

The Infrared Atlas Charts have been quantized to specific levels. Each increase of intensity corresponds to 4K temperature increase if located at the disk center. For example, on IAC 58 Copernicus the crater Hortensius C (26.7°W, 5.9°N) has 4 levels of brightness above the *base* (black) which is an enhancement of between 16K and 20K. The actual digital data indicates Hortensius C has an enhancement of 17.5K. When the enhancement is large there are reading difficulties. Gambart A (18.7°W; 1.0°N) has at least 5 levels above the base, a temperature difference of 20K or greater. The actual digital data in this case indicates 42.1K. The difference (error) is a result of the photographic method, that is, a sufficient number of intensity levels cannot be displayed. Also the hot spot region is so small that the intensity levels are blurred together. The charts, therefore, should be used carefully where 5 levels of intensity

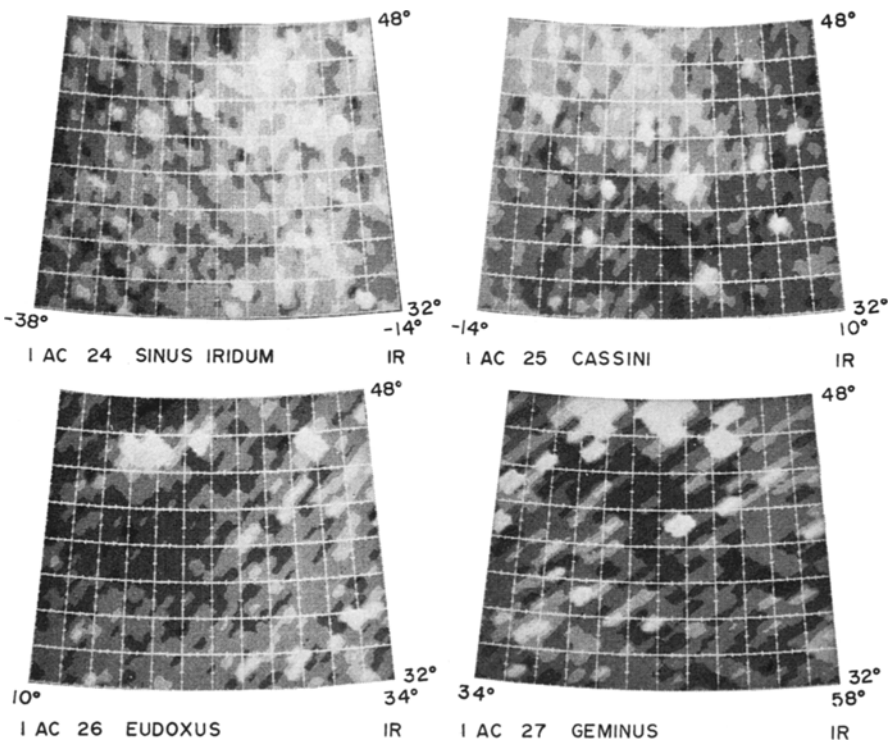

Plate A-II.

are found. A list of the eclipse enhancements for more than 500 hot spots will be published elsewhere.

The selenographic grids are spaced 2° apart with a large tic mark every degree and small tick marks every 0.5 deg. The slight uneveness in the grid is a result of the finite size of the computation interval. Certain distortions occur at large radial distances from the disk center as described in Section 3. The finite size of the sensor and the traverse motion tend to show lineation (see IAC 13 Aristotle). When transforming from an orthographic projection to a Mercator or Lambert projection there is a general curvature appearance caused by stretching what were straight traverse lines (see IAC 80 Langrenus). There was not always a one to one correspondence between the orthographic data when transformed into the Mercator or Lambert projection. This occurred because the same orthographic data point was used several times to fill in different (adjacent) positions. For example in IAC 93 Mare Humorum the southwest perimeter of Mare Humorum is straight while in the original data it appears more rounded. However it must be noted that all these transformation distortions fall within the resolution limit of the infrared photometer. Another positional error encountered frequently is caused by the finite size of the aperture. Any source falling within the instantaneous field of view will be plotted as a point, thus a small hot spot

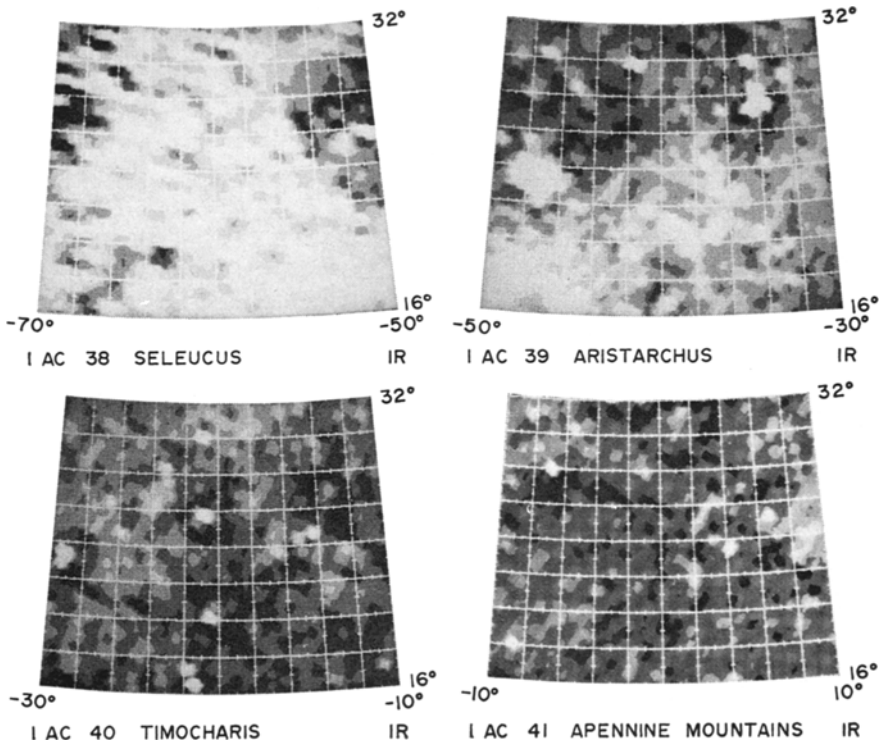

Plate A-III.

on the perimeter of the field of view will appear to be located at the center of the traverse line. This could shift the position by as much as 8 km in a direction perpendicular to the traverse direction. An example of this (see Figure 7) can be seen in IAC 41 where the hot spot associated with a bright crater at (8°.6E; 22°.9N) is shifted to the southwest at (8°.3E; 22°.6N). A similar effect is the elongation of hot spots in a direction perpendicular to the traverse direction. This is caused when successive traverses pass over a hot spot that is smaller than the projected aperture. The hot spot not only is degraded in signal strength but is shifted in position, part to the center of one traverse line and a part to the center of the other traverse line, thus elongating the hot spot. In the majority of cases these errors are easy to detect.

Plate A-I shows IAC 11, 12, 13 and 23. Subsequent Plates A-II through A-XI also show 4 charts each. The charts are labeled with corner coordinates. The darkest level (see IAC 27 and 56 for example) represent no enhancement. Note that IAC 57 Kepler has very little area that is not enhanced, while IAC 95 Purbach has very little area that is enhanced except for the localized hot spots. Since the IR data have been normalized all Infrared Atlas Charts may be compared directly.

The author wishes to say to Dr Harold C. Urey, truly an outstanding 'hot spot' among lunar scientists, "many happy returns on your birthday and best wishes."

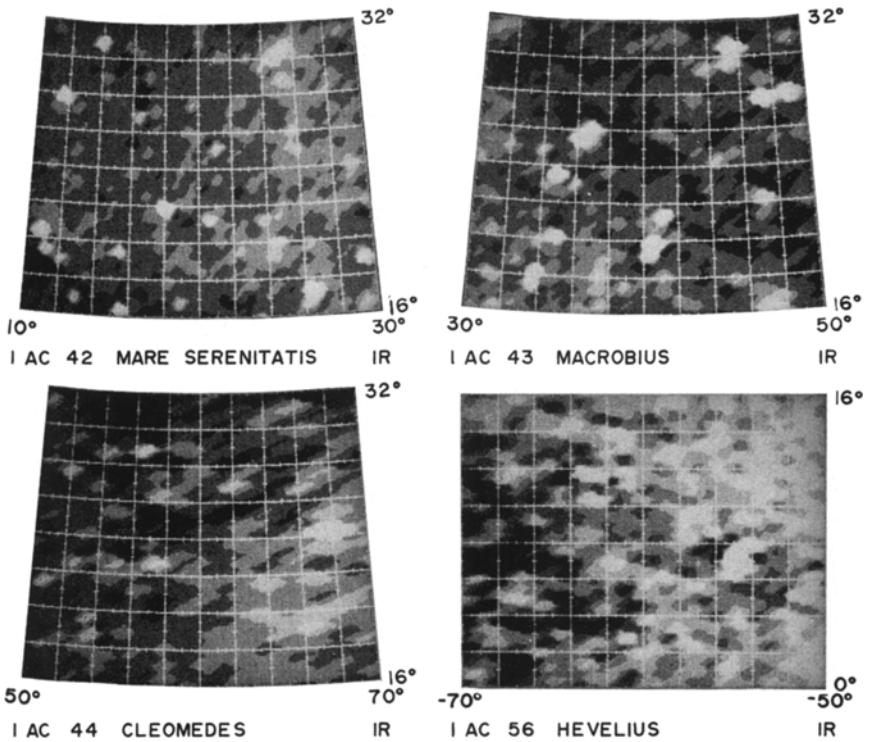

Plate A-IV.

Acknowledgments

The author expresses his gratitude to Dr T. W. Thompson of the Jet Propulsion Laboratories of Pasadena, California, for producing the 44 images that make up this Atlas at the Image Processing Laboratory of JPL. Mr L. A. Hughes of The Boeing Company did the computor data reduction for the tapes that were sent to JPL. The comments of Dr L. B. Ronca and Dr D. R. Criswell were helpful. The photography support of the Manned Spacecraft Center is acknowledged. The author appreciates the opportunity to participate in the Visiting Scientist program at The Lunar Science Institute. The observations and some of the data reduction were done during the period when the author and the late Mr John M. Saari worked together.

Appendix: List of Infrared Atlantes

Infrared atlantes of the Moon have been constructed for small localized regions to the entire disk. These include mappings of the lunar surface at different phases during the day and night-time, and during eclipses. The isothermal contour maps, thermal images, and lists of thermal anomalies are described briefly.

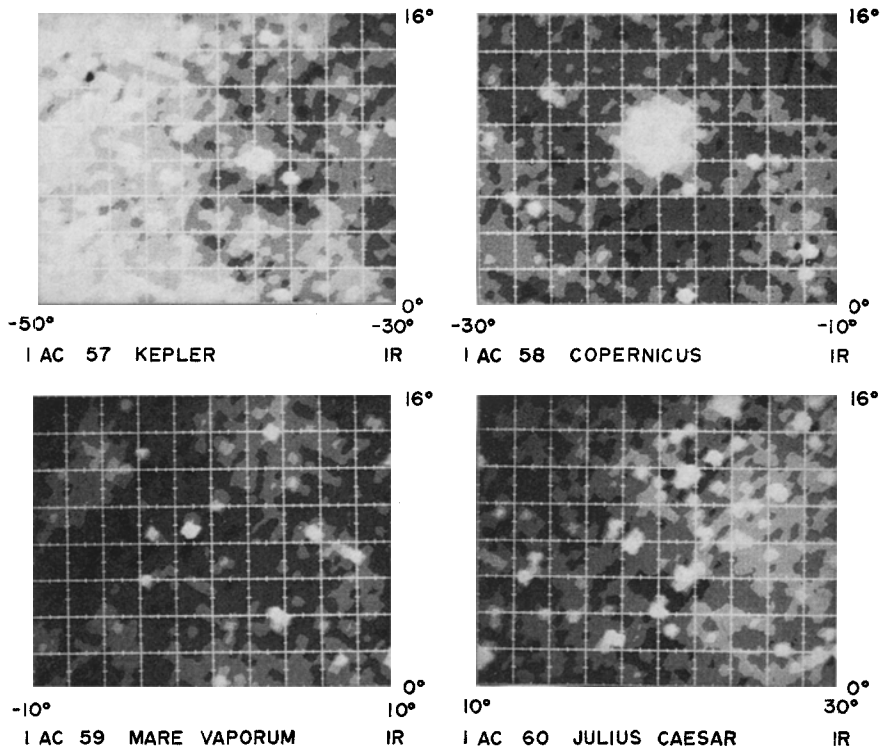

Plate A-V.

(1) (1972) *Infrared and Radar Maps of the Lunar Equatorial Region:* A Mercator projection of the region $\pm 16°$ lat. by $\pm 70°$ long. Grid lines are 5° apart in long. and 10° in lat. with tick marks every degree. Also 3.8-cm and 70-cm radar backscatter maps for the same region at the identical scale and projection are included for comparison (Shorthill, R. W., Thompson, T. W., and Zisk, S. H.: 1972, *The Moon* **3**, 313–317).

(2) (1972) *Infrared Observations on the Eclipsed Moon:* A set of 20 isothermal contour maps constructed from measurements taken during the totality phase of the lunar eclipse of 1964, December 19, $3^h02^m.82$ UT. The contours are overlaid on to the AIC* series of lunar charts. The AIC charts cover the area $\pm 8°$ lat. and $\pm 50°$ long. in 8° lat. by 10° long. sections. The isothermal contour interval is 2K with the maximum and minimum values indicated. The thermal anomalies can be directly related to lunar features.

Also included in this paper is the eclipse isothermal contour map of the entire Earth-side disk with a 2K contour interval. A librated standard orthographic grid facilitates the location of features. The contour lines are sharp but the contour numbers

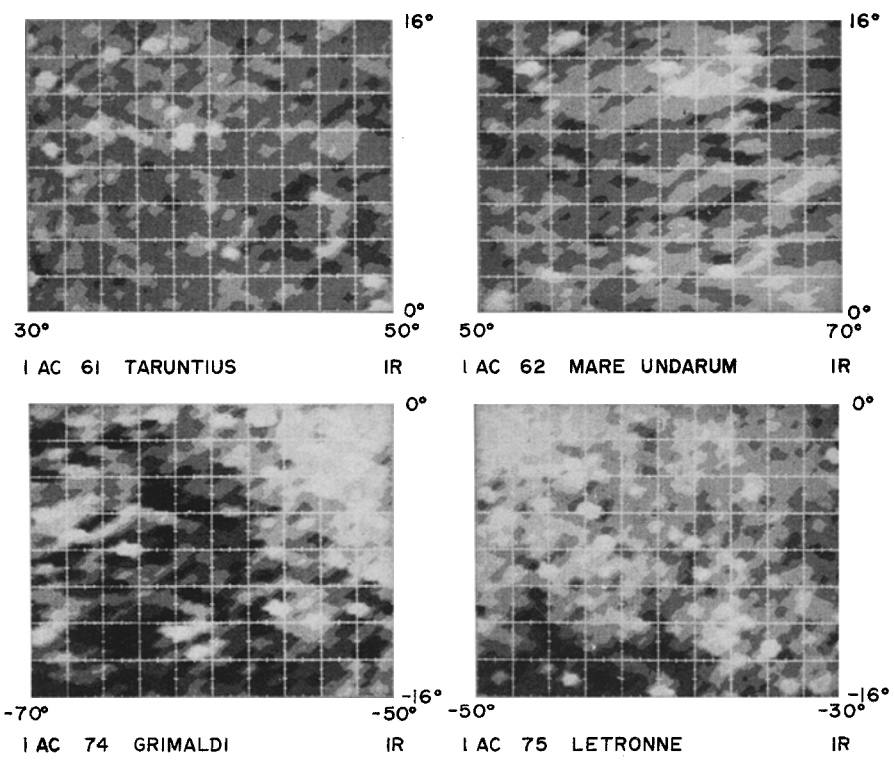

Plate A-VI.

* The AIC maps were produced by the United States Air Force Aeronautical Chart and Information Center, St. Louis, Missouri.

are difficult to read. In addition a list of the 165 thermal anomalies (5 K above environs) in the $\pm 8°$ lat. and $\pm 50°$ long. is annotated (Shorthill, R. W. and Saari, J. M.: 1972, *Adv. Astron. Astrophys.* **9**, 149–200. Also 1972, *Boeing Scientific Research Laboratories Document* D1-82-0778).

(3) (1971) *Infrared Studies of the Lunar Terrain.* I. *The Background Moon:* This paper lists 35 thermal anomalies observed near the limbs during the lunar night. Location and remarks are given for each anomaly. There is also a list of the thermal response over 13 areas of prominent mass concentrations (Allen, D. A.: 1971, *The Moon* **2**, 320–337).

(4) (1971) *Infrared Studies of the Lunar Terrain.* II. *Thermal anomalies:* This report presents an extensive listing of thermal anomalies observed during the lunar night time, 266 in all. For each of the entries coordinates are given along with notes and observing data. Also listed is the location of 7 thermal anomalies at 21 μm wavelength (Allen, David A.: 1971, *The Moon* **2**, 435–462).

(5) (1968) *Infrared Images and an Anomaly of Possible Internal Origin:* One infrared image of 20% of the lunar disk during the lunar eclipse of April 13, 1968 is shown. Also one infrared image of the Humorum region during the late afternoon showing the location of a linear feature in Humorum (Hunt, G. R., Salisbury, J. W., and Vincent, K.: 1968, *Science* **162**, 252–254).

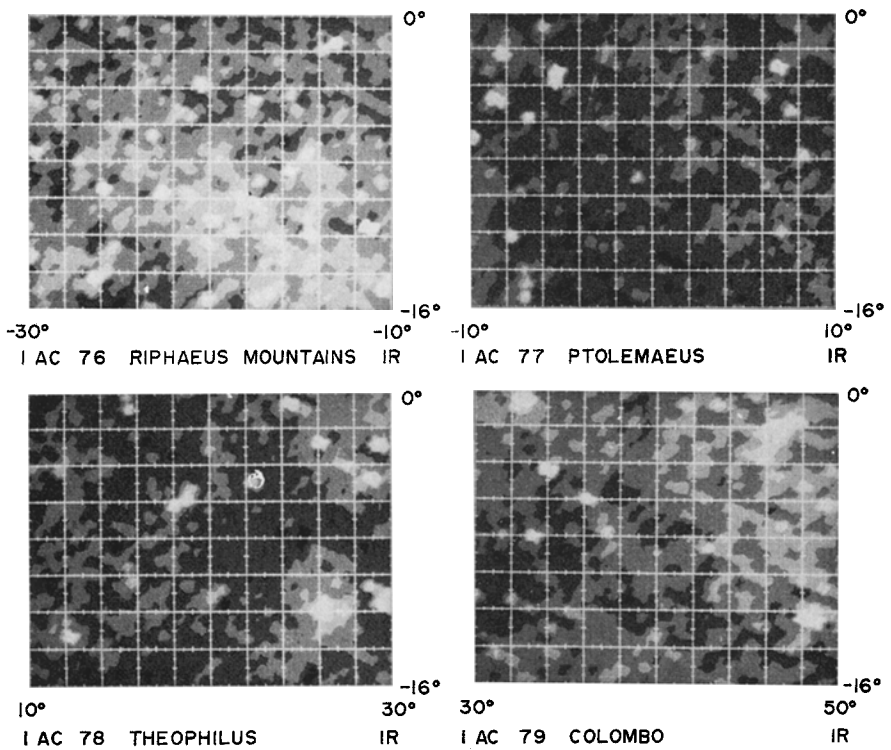

Plate A-VII.

(6) (1968) *Infrared Images of the Eclipsed Moon:* This report shows infrared images made during the total lunar eclipse of April 13, 1968. Five different regions are illustrated covering about 70% of the lunar disk. Several features on each image are called out (Hunt, G. R., Salisbury, J. W., and Vincent, R. K.: 1968, *Sky Telesc.* **36**, 223–225).

(7) (1967) *Isothermal and Isophotic Atlas of the Moon:* A set of isothermal and isophotic charts of the illuminated disk for 23 different phase angles from −124° to 136° are given. The infrared and visible data were obtained simultaneously and each pair of charts are divided into the four quadrants of the lunar disk. The resolution is from $\frac{1}{200}$ to $\frac{1}{250}$ of the lunar disk diameter (8 to 10″). The contour intervals are 1 to 3 K in the infrared and in the visible 1% to 4% of the full Moon brightness. The contours are overlaid with the standard orthographic grid so that features are easily identifiable. This atlas will be revised and published in a scientific journal in 1973 (Saari, J. M. and Shorthill, R. W.: 1967, *NASA Contractor Report NASA CR-855*, 1–186).

(8) (1967) *Reconnaissance of Infrared Emission from the Lunar Night-time Surface:* This paper lists 110 thermal anomalies observed during the lunar night-time. Locations are given to the nearest degree along with observational data. An isothermal contour

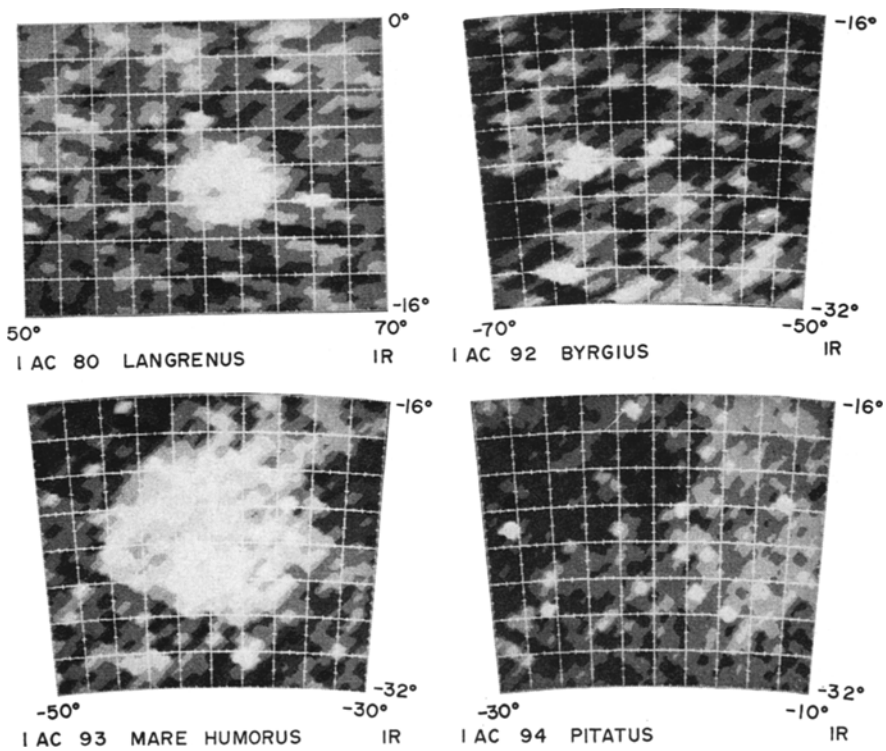

Plate A-VIII.

chart of the night-time hemisphere of the third quarter Moon is shown. Some of the thermal anomalies are marked on the chart (Wildey, R. L., Murray, B. C., and Westphal, J. A.: 1967, *J. Geophys. Res.* **72**, 3743–3749).

(9) (1966) *Hot Spots on the Moon:* Included in this paper is a chart of the Earth side disk showing the location of 330 thermal anomalies measured during the total lunar eclipse of 1964, December 19. The ability to locate features is limited, since only the maria are outlined and 9 craters are indicated (Saari, John M. and Shorthill, Richard W.: 1966, *Sky Telesc.* **31**, 3–7).

(10) (1966) *Isotherms in the Equatorial Region of the Totally Eclipsed Moon:* An isothermal contour chart ($\pm 10°$ lat. and $\pm 90°$ long.) made from measurements of the total lunar eclipse December 19, 1964, $3^h2^m.8$ UT. The chart has a selenographic grid with 1° increments in latitude and longitude. Between $\pm 5°$ lat. 55 thermal anomalies are indicated (Saari, J. M. and Shorthill, R. W.: 1966, *Boeing Scientific Research Laboratories Document* D1-82-0530, 1–3).

(11) (1966) *Infrared and Visible Images of the Eclipsed Moon of December 19, 1964:* A set of 17 infrared and visible images made during the eclipse and during the full Moon. Each image covers the lunar disk. Features can be identified by comparing the visible and the infrared image (Saari, J. M., Shorthill, R. W., and Deaton, T. K.:

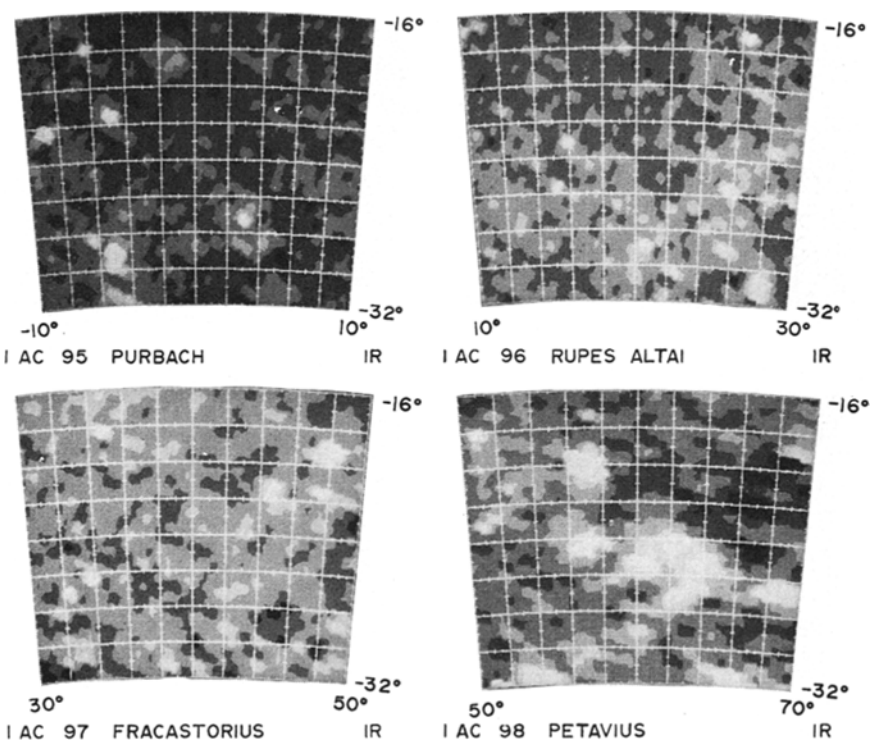

Plate A-IX.

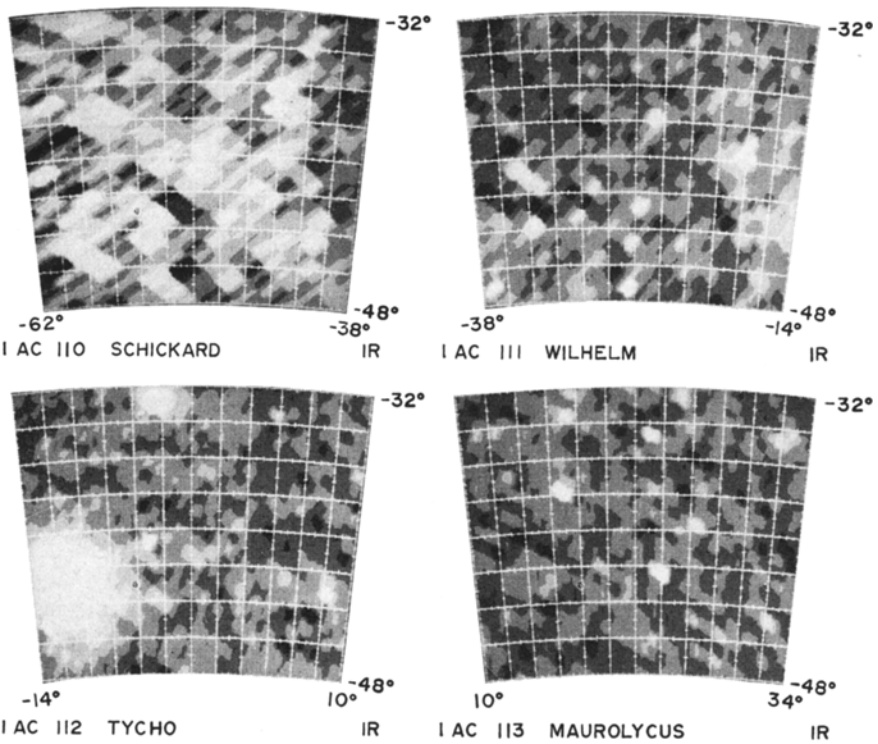

Plate A-X.

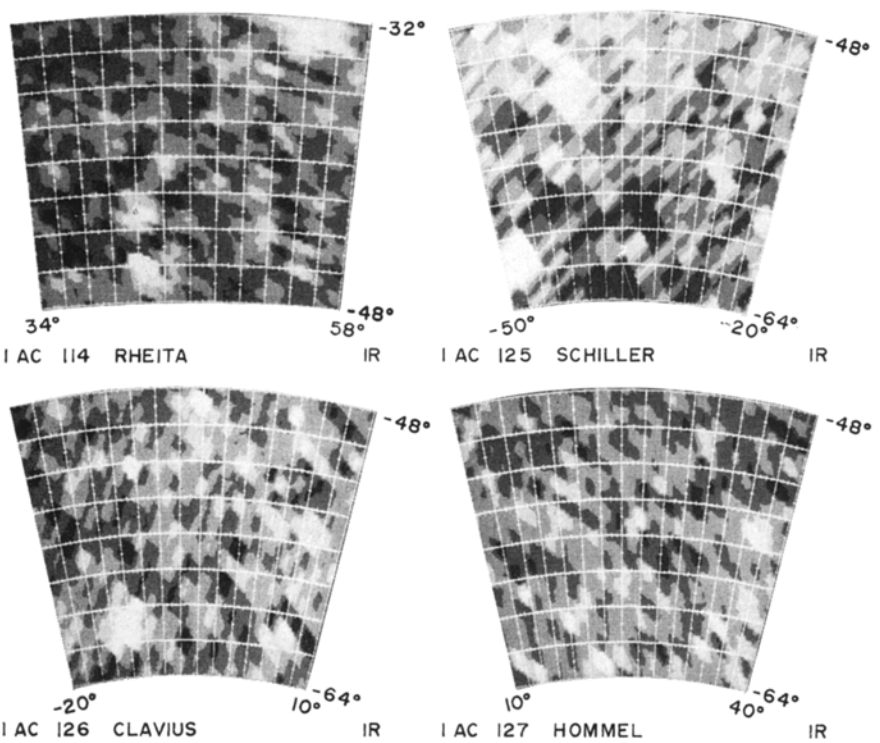

Plate A-XI.

1966, *Icarus* **5**, 635–659. Also 1966, *Boeing Scientific Research Laboratories Document* D1-82-0533, 1–40).

(12) (1965) *Nonuniform Cooling of the Eclipsed Moon: A Listing of Thirty Prominent Anomalies:* A list of the most prominent eclipse thermal anomalies (30 hot spots), corrected for the effect of sensor resolution. All these craters have diameters less than the sensor resolution (Shorthill, R. W. and Saari, J. M.: 1965, *Science* **150**, 210–212).

(13) (1963) *Isotherms of Crater Regions on the Illuminated and Eclipsed Moon:* A set of isothermal contours for eleven different craters around full Moon. Four of these craters were also mapped during a total eclipse of September 5, 1960. The resolution was $\frac{1}{250}$ of the lunar disk (8″). The contour interval was 1 K (full Moon) and 5 K (eclipsed Moon). Features can be identified. Some of the charts are overlayed on portions of the 'Photographic Lunar Atlas', (University of Chicago press, Chicago, G. P. Kuiper (ed.), 1960). (Saari, J. M. and Shorthill, R. W.: 1963, *Icarus* **2**, 115–136; also 1962, 'Infrared Mapping of Lunar Craters During the Full Moon and Total Eclipse of September 5, 1960', *Boeing Scientific Research Laboratories Document* D1-82-0276).

(14) (1960) *Isothermal Contours of the Moon:* A set of isothermal contour charts of the illuminated Moon for nine different phases. The resolution was $\frac{1}{72}$ of the lunar disk. The contour interval was 10–30 K. Because of the limited resolution and the absences of selenographic grids correlation with surface features is not possible (Geoffrion, A. R., Korner, M., and Sinton, W. M.: 1960, *Lowell Observatory Bulletin No. 106* **V**, No. 1, 1–15).

References

Allen, D. A.: 1971a, *The Moon* **2**, 320–337.
Allen, D. A.: 1971b, *The Moon* **2**, 435–462.
Mendell, W. W. and Low, F. J.: 1972, *The Moon* **4**, 18–27.
Murray, B. C. and Wildey, R. L.: 1964, *Astrophys. J.* **139**, 734–750.
Roelof, E. C.: 1968, *Icarus* **8**, 138–159.
Samaha, A. H.: 1967, *Measure of the Moon*, D. Reidel Publishing Co., pp. 78–88.
Saari, J. M. and Shorthill, R. W.: 1963, *Icarus* **2**, 115–136.
Saari, J. M. and Shorthill, R. W.: 1967, 'Isothermal and Isophotic Atlas of the Moon', CR-855, NASA, 1–186.
Shorthill, R. W.: 1972, in John W. Lucas (ed.), 'The Infrared Moon', Chapter 1 in *Lunar Thermal Characteristics*, AIAA Progress Series Volume (in press).
Shorthill, R. W., Borough, H. C., and Conley, J. M.: 1960, *Publ. Astron. Soc. Pacific* **72**, 481–485.
Shorthill, R. W. and Saari, J. M.: 1965a, *Ann. N.Y. Acad. Sci.* **123**, 722–739.
Shorthill, R. W. and Saari, J. M.: 1965b, *Science* **150**, 210–212.
Shorthill, R. W., Saari, J. M., Baird, F. E., and Le Compte, J. R.: 1970, Contract NAS 9-9794 Final Report, 1–447.
Shorthill, R. W. and Saari, J. M.: 1972, *Adv. Astron. Astrophys.* **9**, 149–201.
Shorthill, R. W., Thompson, T. W., and Zisk, S. H.: 1972, *The Moon* **3**, 313–317.
Thompson, T. W.: 1973, 'Radar Atlas of the Moon', *The Moon* (in press).
Thompson, T. W., Masursky, H., Shorthill, R. W., Zisk, S. H., and Tyler, G. L.: 1970, *The Lunar Science Institute Contribution No. 16*, 1–45.
Winter, D. F.: 1966a, *Intern. J. Heat Transf.* **9**, 527–532.
Winter, D. F.: 1966b, *Icarus* **5**, 551–553.
Winter, D. F.: 1967, *Icarus* **6**, 229–235.
Winter, D. F.: 1970, *Radio Sci.* **5**, 229–240, and (Errata), 5.

Winter, D. F. and Saari, J. M.: 1969, *Astrophys. J.* **156**, 1135–1151.
Zisk, S. H., Caar, M. H., Masursky, H., Shorthill, R. W., and Thompson, T. W.: 1971, *Science* **173**, 808–812.
Zisk, S. H., Masursky, H., Milton, D. J., Schaber, G. G., Shorthill, R. W., and Thompson, T. W.: 1972, *90-Day Mission Report Apollo 16* (to be published).